BOUNDARY CORRECTIONS FOR A THREE-COIL CONDUCTIVITY/VELOCITY PLASMA PROBE

by Edward W. Vendell

Ames Research Center
Moffett Field, Calif.

BOUNDARY CORRECTIONS FOR A THREE-COIL

CONDUCTIVITY/VELOCITY PLASMA PROBE

By Edward W. Vendell

Ames Research Center
Moffett Field, Calif.

NATIONAL AERONAUTICS AND SPACE ADMINISTRATION

TABLE OF CONTENTS

BOUNDARY CORRECTIONS FOR A THREE-COIL

CONDUCTIVITY/VELOCITY PLASMA PROBE*

By Edward W. Vendell

Ames Research Center

SUMMARY

A three-coil plasma probe that measures both the electrical conductivity and velocity of laboratory plasmas having low magnetic Reynolds numbers has been developed and tested by Rossow and Posch. As a first approximation, it was assumed that the plasma boundary was far from and much larger than the probe. At the suggestion of V. J. Rossow, the present work was undertaken to extend the previous theory by deriving factors that correct for the presence of cylindrical boundaries. As a check on this numerical work, several computed values were compared with electrical conductivity measured in cylinders of acid. Since the agreement was satisfactory, the boundary correction factors were used to reduce data taken as the probe was swept through an argon plasma generated by a constricted-arc wind tunnel. These resultant profiles represent local conductivity and velocity values for a free plasma jet having a cylindrical boundary. It was found that the raw data underestimates conductivity and overestimates velocity.

INTRODUCTION

The measurement of the electrical conductivity and velocity of high-temperature laboratory plasmas has necessitated the modification of traditional immersible transducers. Instruments, such as pitot tubes and thermocouples, must be designed to withstand high heat-flux rates and to function properly in an ionized environment without greatly perturbing the medium. In the past, several external measurement techniques have been developed to determine electron and ion temperatures, particle number densities, and the total electron collision frequency. These properties have been used to infer values of the transport coefficients by means of appropriate formulae.

Measurements within the plasma stream are desirable for checking the external methods and for obtaining, if possible, local values. Consequently, many conductivity instruments have been conceived (see, e.g., refs. 1-16), a few of which are immersible (see refs. 4, 5, 11, and 16). A similar situation exists for velocity measurement techniques (see, e.g., refs. 12, 14, and

---

16-20). For a brief review and comparison of conductivity and velocity techniques, the reader is referred to reference 21.

The present work is based on a design by Rossow and Posch (ref. 16) of an immersible three-coil electrical conductivity/velocity probe that represents a significant improvement upon previous methods because it minimizes the heat-flux sensitivity (refs. 4 and 5) and large flow-perturbation problems (ref. 4) of other designs and because data taken with this instrument can be reduced to obtain local values of conductivity and velocity. Briefly, this device consists of three small coils, one primary and two secondary. The alternating current in the primary coil creates an oscillating magnetic dipole field. The secondary coils are located in spatial positions such that the voltage induced on one coil is linearly related to the conductivity while the voltage on the other coil is linearly related to the conductivity-velocity product. Thus the data taken as the probe sweeps across a diameter of a plasma jet may be used to determine both conductivity and velocity profiles.

In the theoretical analysis of most magnetofluidmechanic problems, the magnetic Reynolds number, $R_m = \sigma\mu U l$, indicates the relative magnitudes between the impressed and induced magnetic fields. In this definition σ is the electrical conductivity, μ is the magnetic permeability, U is the speed, and l is some characteristic length. If R_m is small, reference 22 shows that the induced magnetic field is also small compared to the impressed field. Then the analysis can be greatly simplified by the use of a power series expansion in R_m since only first-order terms need be considered. This approach was used in the analysis of Rossow and Posch because R_m is small for most plasmas generated by electric arcs; the probe design of reference 16 was tested in a constricted-arc wind tunnel where R_m ranged from 10^{-4} to 10^{-1}. Therefore, the neglect of terms of order R_m^2 was reasonable and these terms will also be omitted in the present analysis.

The theory of Rossow and Posch also assumed an unbounded plasma having uniform electrical conductivity and velocity. The principal purpose of this paper is to present theoretical modifications which will remove these restrictions for the case of a free plasma jet having a cylindrical boundary.

Accordingly, modifications of the unbounded field theory that are necessary whenever the three-coil probe nears a plasma boundary are derived and computed numerically. Initially, the conductivity σ and velocity U are assumed to be constant inside the jet of radius R and zero elsewhere. From this idealized model, the modifications are derived and presented graphically in the form of boundary correction factors. These theoretical correction factors are compared with experimental results obtained by immersing a three-coil probe in a deep plastic cylinder filled with an electrolyte.

Then the correction factors are used to develop a method for computing the local conductivity and velocity of a plasma stream from data which varied continuously across a low-density argon plasma jet generated by a constricted-arc wind tunnel. The method is then applied to a typical data record and the resulting conductivity and velocity profiles are presented and discussed.

$\underset{\sim}{A}$	vector potential function
$\underset{\sim}{B}$	magnetic induction vector
$\underset{\sim}{B}_p$	primary dipole magnetic induction vector
$\underset{\sim}{b}_t, \underset{\sim}{b}_{||}$	first-order magnetic induction vectors
c_Σ	conductivity calibration constant
c_Υ	velocity calibration constant
$\underset{\sim}{D}$	electric displacement vector
$\underset{\sim}{E}$	electric field intensity vector
e	electron charge
$\underset{\sim}{H}$	magnetic field intensity vector
I_p	total current, primary coil
$\underset{\sim}{J}$	current density vector
$\underset{\sim}{J}_t, \underset{\sim}{J}_{||}$	first-order current density vectors
n_p	number of turns, primary coil
n_Σ	number of turns, Σ-coil
n_Υ	number of turns, Υ-coil
p	subscript referring to primary-coil parameters
P	dimensionless radial distance to location of primary coil ($P = \rho/R$)
R	radius of a cylindrical region
R_m	magnetic Reynolds number
r	distance in spherical coordinates
r_p	characteristic radius, primary coil
r_Σ	characteristic radius, Σ-coil
r_Υ	characteristic radius, Υ-coil
S	dimensionless coil spacing parameter ($S = y_\Sigma/R$)

t	subscript refers to first-order fields caused by σ
$\underset{\sim}{U}$	velocity vector
$U_{\|}$	axial velocity component
X,Y,Z	dimensionless Cartesian coordinates
x,y,z	Cartesian coordinates
y_Σ	radial distance from primary coil to either secondary coil
z	axial coordinate
ϵ	dielectric constant
Θ_Σ	boundary correction factor for σ
Θ_Y	boundary correction factor for $\sigma U_{\|}$
θ	azimuthal coordinate
μ	magnetic permeability
ρ	radial distance in cylindrical coordinates
$(\ )_\Sigma$	conductivity-coil parameters
σ	electrical conductivity
$(\ )_Y$	conductivity velocity coil parameters
Φ_Σ	signal induced on Σ-coil
$\Phi_{\Sigma\infty}$	signal induced on Σ-coil in an infinite medium
Φ_Y	signal induced on Y-coil
$\Phi_{Y\infty}$	signal induced on Y-coil in an infinite medium
ψ	stream function for current density vector
ω	frequency of impressed power
$(\ )_{\|}$	first-order fields caused by $\sigma U_{\|}$

A THREE-COIL CONDUCTIVITY/VELOCITY PROBE

Rossow and Posch (ref. 16) have developed and tested an immersible, three-coil plasma probe that represents a significant improvement upon

previous techniques because it is capable of determining local electrical conductivity and velocity values without greatly perturbing the flow and because it can be used in such a manner that heat-flux sensitivity is negligible. Since the present work is based on the probe design of Rossow and Posch, selected material from reference 16 will be reviewed in this section.
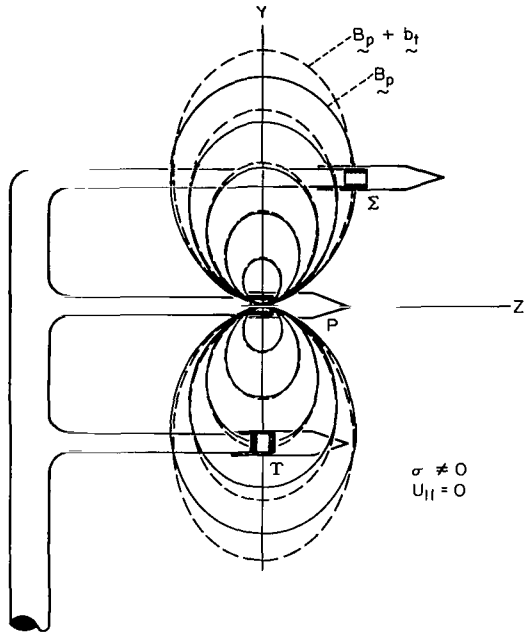

Figure 1.- Perturbation of $\underset{\sim}{B}_p$ caused by a conducting fluid at rest.

Figure 2.- Perturbation of $\underset{\sim}{B}_p$ caused by a moving conducting fluid.
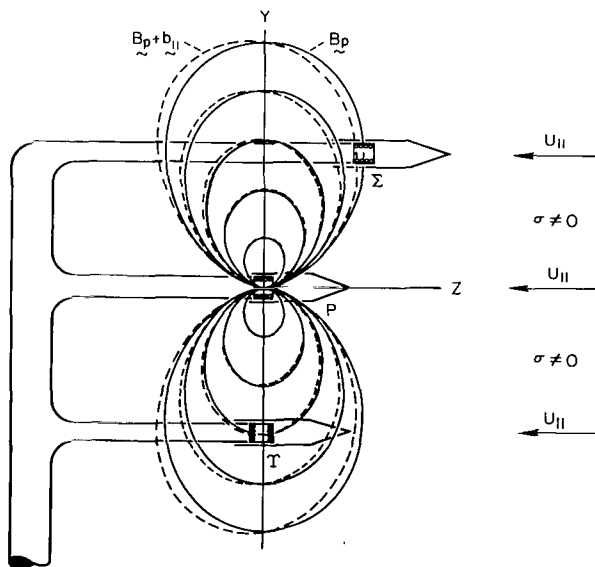
The basic concepts of the instrument are illustrated in figures 1 and 2 which were prepared by superposition of the probe onto figures 2 and 3 of reference 16. Figure 1 represents the principle by which conductivity is measured. Three small coils labeled P for primary, Σ for conductivity, and Y for velocity, lie in the same plane $(x = 0)$ and are mounted on support rods in such a way that the axes of the Σ- and P-coils are parallel to the z axis while the axis of the Y-coil is parallel to the y axis.

In the absence of a conducting or a dielectric medium, the pulsating current in the primary coil produces magnetic flux which may be approximated by an oscillating ideal magnetic dipole field. The solid lines labeled $\underset{\sim}{B}_p$ indicate the shape of the lines of force for the primary dipole field at an instant in time. Under these circumstances, the primary field, having no axial component, produces no flux linkage at either the Σ-coil or the Y-coil. However, in the presence of a conducting, quiescent medium, the primary magnetic field induces currents which, in turn, create a perturbation magnetic field designated $\underset{\sim}{b}_t$. The dotted lines indicate an instantaneous position of the lines of force for the resultant magnetic field which produces flux linkage at the Σ-coil; however, the Y-coil remains free of flux linkage because of its orientation.

Similarly, in figure 2, the dotted lines indicate a particular instantaneous position of the lines of force for the resultant magnetic field which is the sum of the primary

5

field $\underset{\sim}{B}_p$ and a perturbation field $\underset{\sim}{b}_{||}$ caused by the motion of a conducting fluid across the primary lines of force. As the sketch shows, the resultant field produces flux linkage at the Y-coil while the Σ-coil flux linkage is zero for such a disturbance.

Since the perturbation fluxes at the two secondary coils are time dependent, Faraday's law of induction implies that the potential output of the Σ-coil will be proportional to the magnitude of the z component of the field perturbation caused by the conductivity σ, and the potential output of the Y-coil will be proportional to the magnitude of the y component of the field perturbation caused by the product of the conductivity σ and velocity $U_{||}$ or $\sigma U_{||}$.

The theoretical analysis of Rossow and Posch begins with Maxwell's equations

$$\underset{\sim}{\nabla} \cdot \underset{\sim}{B} = 0 , \qquad \underset{\sim}{\nabla} \cdot \underset{\sim}{E} = 0 \tag{1}$$

$$\underset{\sim}{\nabla} \times \underset{\sim}{B} = \mu \underset{\sim}{J} \tag{2}$$

$$\underset{\sim}{\nabla} \times \underset{\sim}{E} = -\frac{\partial \underset{\sim}{B}}{\partial t} \tag{3}$$

the simplified Ohm's law

$$\underset{\sim}{J} = \sigma(\underset{\sim}{E} + \underset{\sim}{U} \times \underset{\sim}{B}) \tag{4}$$

the conservation of charge equation for a neutral plasma

$$\underset{\sim}{\nabla} \cdot \underset{\sim}{J} = 0 \tag{5}$$

and the Coulomb or transverse-gage condition

$$\underset{\sim}{\nabla} \cdot \underset{\sim}{A} = 0 \tag{6}$$

In these equations $\underset{\sim}{E}$ is the electric field intensity vector, $\underset{\sim}{B}$ is the magnetic induction vector, $\underset{\sim}{J}$ is the current density vector, $\underset{\sim}{U}$ is the plasma velocity vector, σ is the electrical conductivity, μ is the permeability, and $\underset{\sim}{A}$ is a vector potential function such that

$$\underset{\sim}{B} = \underset{\sim}{\nabla} \times \underset{\sim}{A} \tag{7}$$

To obtain a solution for these equations, Rossow and Posch imposed the following restrictions:

1. The flow field is unbounded.

2. The electrical conductivity and velocity are taken to be constant over the entire flow field.

3. The only applied field is $\underset{\sim}{B}_p$ which is the magnetic field created by the oscillating current in the primary coil.

4. Since the magnitude of $\underset{\sim}{B}_p$ is less than 10^{-2} gauss, the assumption of scalar electrical conductivity is justifiable. (In the presence of large applied fields, the conductivity of a plasma assumes a tensorial form.)

5. The small magnitude of $\underset{\sim}{B}_p$ also justifies the representation of the resultant magnetic field, $\underset{\sim}{B}$, as a power series expansion in the magnetic Reynolds number, R_m. As mentioned previously, typical values of R_m for low density constricted-arc wind tunnels range from 10^{-4} to 10^{-1} so that neglecting terms of order $R_m{}^2$ is reasonable. (See ref. 22 for details on series expansions in the magnetic Reynolds number.)

6. Perturbations of the stream caused by the presence of the probe are neglected.

7. In equation (2) the displacement current term is neglected. Omission of this term is justified in reference 21.

As a zeroth-order approximation for $\underset{\sim}{B}$, Rossow and Posch used the primary dipole field $\underset{\sim}{B}_p$ that would be produced by an idealized primary coil in free space. The vector potential $\underset{\sim}{A}_p$ for such a field is well known and appears on page 237 of reference 23 as

$$\underset{\sim}{A}_p(x,y,z,t) = \frac{\mu}{4\pi} \underset{\sim}{m} \times \underset{\sim}{\nabla}\left(\frac{1}{r}\right) \tag{8}$$

where $\underset{\sim}{m}$ is the magnetic dipole moment of the idealized primary coil located at $(x,y,z) = (0,0,0)$, and $r = (x^2 + y^2 + z^2)^{1/2}$. Thus, equation (7) yields the solution

$$\underset{\sim}{B}_p = \underset{\sim}{\nabla} \times \underset{\sim}{A}_p \tag{9}$$

Since $\underset{\sim}{B}_p$ is time dependent, equation (3) requires the existence of an associated electric field, denoted by subscript t, such that

$$\underset{\sim}{\nabla} \times \underset{\sim}{E}_t = -\frac{\partial \underset{\sim}{B}_p}{\partial t} \tag{10}$$

and this equation may be solved for $\underset{\sim}{E}_t$.

Equation (4) suggests that the total current may be considered the sum of two components, the first of which is

$$\underset{\sim}{J}_t = \sigma \underset{\sim}{E}_t \tag{11}$$

and the second is

$$\underset{\sim}{J}_{\parallel} = \sigma \underset{\sim}{U} \times \underset{\sim}{B}_p = \sigma U_{\parallel}\underset{\sim}{k} \times \underset{\sim}{B}_p \tag{12}$$

where $\underset{\sim}{U} = U_{\parallel}\underset{\sim}{k}$, as in figure 2 with the unit vectors $\underset{\sim}{i}$, $\underset{\sim}{j}$, $\underset{\sim}{k}$ directed in the positive x, y, z directions, respectively. The first component, $\underset{\sim}{J}_t$, is caused by the application of an electric field, $\underset{\sim}{E}_t$, to a stationary conducting fluid. The second component, $\underset{\sim}{J}_{\parallel}$, arises from the motion $U_{\parallel}\underset{\sim}{k}$ of a conducting fluid across lines of force, $\underset{\sim}{B}_p$.

Rossow and Posch continued the analysis by using equation (2) to solve for the first-order perturbation fields $\underset{\sim}{b}_t$ and $\underset{\sim}{b}_{\parallel}$ that accompany $\underset{\sim}{J}_t$ and $\underset{\sim}{J}_{\parallel}$. Thus, the resultant magnetic field, including first-order terms only, is

$$\underset{\sim}{B} = \underset{\sim}{B}_p + \underset{\sim}{b}_t + \underset{\sim}{b}_{\parallel} \tag{13}$$

This equation, together with equations (2), (3), and (4), could be used to solve for currents and perturbation fields of higher order in R_m. However, as previously mentioned, the terms of higher order may be neglected in the present case because R_m is small.

For future reference, the following solutions are listed from reference 16:

$$\underset{\sim}{B}_p = -m \cos \omega t \left[\underset{\sim}{i}\ \frac{3xz}{r^5} + \underset{\sim}{j}\ \frac{3yz}{r^5} + \frac{\underset{\sim}{k}}{r^3}\left(\frac{3z^2}{r^2} - 1 \right) \right] \tag{14}$$

$$\underset{\sim}{E}_t = -\omega m \sin \omega t\, \underset{\sim}{\nabla} \times \left(\frac{\underset{\sim}{k}}{r} \right) \tag{15}$$

$$\underset{\sim}{J}_t = -\sigma \omega m \sin \omega t \left[\underset{\sim}{i}\left(\frac{-y}{r^3} \right) + \underset{\sim}{j}\left(\frac{x}{r^3} \right) \right] \tag{16}$$

$$\underset{\sim}{J}_{\parallel} = 3 U_{\parallel} m \cos \omega t \left[\underset{\sim}{i}\ \frac{yz}{r^5} - \underset{\sim}{j}\ \frac{xz}{r^5} \right] \tag{17}$$

$$\underset{\sim}{b}_t = -\frac{\sigma \mu \omega m}{2} \sin \omega t \left[\underset{\sim}{i}\ \frac{xz}{r^3} + \underset{\sim}{j}\ \frac{yz}{r^3} + \underset{\sim}{k}\ \frac{r^2 + z^2}{r^3} \right] \tag{18}$$

$$\underset{\sim}{b}_{\parallel} = \frac{\sigma \mu U_{\parallel} m}{2} \cos \omega t \left[1 - \frac{3z^2}{r^2} \right]\left[\underset{\sim}{i}\ \frac{x}{r^3} + \underset{\sim}{j}\ \frac{y}{r^3} + \underset{\sim}{k}\ \frac{z}{r^3} \right] \tag{19}$$

$$m = (n_p r_p^2)\mu I_p / 4 \tag{20}$$

where I_p is the peak current supplied at frequency ω to the n_p-turn primary coil whose characteristic radius is r_p.

Equations (14) through (20), plus Faraday's law of induction, suggest that locations and orientations of the Σ- and Y-coils may be selected so as to eliminate unwanted magnetic flux linkage. Faraday's law states that the potential Φ_s induced on a secondary anywhere in the flow field may be approximated by

$$\Phi_s = -\pi n_s r_s^2 \frac{\partial}{\partial t} (\underset{\sim}{B} \cdot \underset{\sim}{N}_s) \tag{21}$$

where r_s is the characteristic radius of the n_s-turn secondary, $\underset{\sim}{B}$ is the resultant field evaluated at the center of the coil, and $\underset{\sim}{N}_s$ is a unit vector parallel to the axis of the coil. Thus, if the center of the Σ-coil is located at $(x,y,z) = (0,y_\Sigma,y_\Sigma/\sqrt{2})$ and is oriented so that $\underset{\sim}{N}_\Sigma = \underset{\sim}{k}$, equations (18) and (21) may be combined to obtain

$$\Phi_{\Sigma\infty} = (n_\Sigma r_\Sigma^2)(n_p r_p^2)(\mu\omega)^2 \frac{\pi I_p \sigma}{6\sqrt{3/2}\, y_\Sigma} \cos \omega t \tag{22}$$

where ∞ refers to an unbounded medium and t is time. Similarly, if the center of the Y-coil is located at $(x,y,z) = (0,-y_\Sigma,0)$ so that $\underset{\sim}{N}_Y = \underset{\sim}{j}$, then the potential induced on the Y-coil in an unbounded medium will be

$$\Phi_{Y\infty} = -(n_Y r_Y^2)(n_p r_p^2) \frac{\mu^2 \omega\pi I_p \sigma U_{||}}{8 y_\Sigma^2} \sin \omega t \tag{23}$$

Thus, equation (22) indicates that $\Phi_{\Sigma\infty}$ is linearly related to σ and equation (23) displays the linear relationship between $\Phi_{Y\infty}$ and $\sigma U_{||}$.

Either one of the two calibration methods given in reference 16 may be used to present equations (22) and (23) in the equivalent form

$$\frac{\Phi_{\Sigma\infty}}{\sigma} = C_\Sigma \tag{24}$$

and

$$\frac{\Phi_{Y\infty}}{\sigma U_{||}} = C_Y \tag{25}$$

where the calibration constants C_Σ and C_Y are functions of the various probe parameters as well as the associated electronic circuitry. It is convenient to compute C_Σ and C_Y so that $\Phi_{\Sigma\infty}$ and $\Phi_{Y\infty}$ represent peak-to-peak values as determined from an oscilloscope data record.

In the next section equations (24) and (25) will be further modified by the introduction of factors that correct for the presence of a cylindrical boundary.

9

FIELD EQUATIONS FOR A CYLINDRICAL CONDUCTING FLUID

As mentioned above, the theory of Rossow and Posch (16) decoupled the perturbation magnetic fields by neglecting terms of order R_m^2, assumed σ and $U_{\parallel}$ to be constant and uniform, and considered only an unbounded medium. This section presents modifications of the previous theory by recognizing the presence of a cylindrical boundary of radius R such that the plasma occupies the region

$$x^2 + y^2 \leq R^2 \; ; \qquad -\infty < z < \infty$$

Also, the position of the probe will not be restricted to the center of the cylindrical region. Furthermore, for this part of the analysis it is assumed that σ and $U_{\parallel}$ are constant and uniform in the region occupied by the plasma and that these quantities vanish elsewhere. The present analysis will also ignore terms of order R_m^2, the displacement current, and relativistic effects. The only applied field is $\underset{\sim}{B}_p$, which is caused by the oscillating current in the primary coil, and this field, being of the order 10^{-2} gauss, is so small that the assumption of scalar electrical conductivity is justified. Finally, as above, perturbations of the stream caused by the presence of the probe are neglected.

Electrical Conductivity

The analysis begins with a consideration of the basic equations which are identical, except for the boundary conditions, to equations (1) through (7).

Because σ and $U_{\parallel}$ vanish outside the cylinder, the two boundary conditions on the current density vector are

$$\underset{\sim}{J} = \underset{\sim}{0} \qquad \text{whenever} \quad x^2 + y^2 > R^2 \tag{26}$$

$$\underset{\sim}{J} \cdot \underset{\sim}{N}_{\perp} = 0 \qquad \text{for} \quad x^2 + y^2 = R^2 \tag{27}$$

where the unit vector, $\underset{\sim}{N}_{\perp}$, is perpendicular to the cylindrical boundary.

If equation (7) is substituted into equation (2), the result will be

$$\underset{\sim}{\nabla} \times \underset{\sim}{\nabla} \times \underset{\sim}{A} = \mu \underset{\sim}{J} \tag{28}$$

and if this expression is expanded so that equation (6) may be applied, the final result will be

$$\underset{\sim}{\nabla}^2 \underset{\sim}{A} = -\mu \underset{\sim}{J} \tag{29}$$

where it is understood that the Laplacian operates on each rectangular component of $\underset{\sim}{A}$. Equation (29) represents a condensation of the three Maxwell equations. Therefore, the problem reduces to the solution of equations (4) and (29) subject to the boundary conditions given by equations (26) and (27).

Equation (29) has a unique solution and it may be solved by finding a Green's function or by an equivalent technique, the method of images (see, e.g., ch. 2, ref. 24). The latter method was chosen because it appears to be a simpler approach and it makes use of equations (14) through (20).

It is also convenient to use an analogy based on the steady, two-dimensional flow of an incompressible fluid for which there exists a potential function Ψ, called the stream function, such that the velocity field $\underset{\sim}{U}$ is given by

$$\underset{\sim}{U} = \underset{\sim}{\nabla} \times \underset{\sim}{\hat{k}}\Psi \tag{30}$$

An important property of the stream function is the fact that lines of constant Ψ are streamlines.

This analogy may be used to represent any two-dimensional current density vector field as

$$\underset{\sim}{J} = \underset{\sim}{\nabla} \times \underset{\sim}{\hat{k}}\psi \tag{31}$$

with the convenient property that current paths or loops coincide with lines of constant ψ.
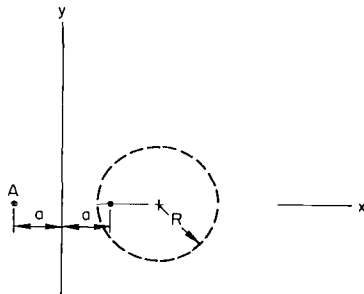
Figure 3.- Coil and image system locations.

Returning to the method of images, consider the geometry of figure 3, where the medium is assumed to be unbounded, at rest, and of uniform and constant σ. If the real coil is located at $(x,y,z) = (a,0,0)$, an image system of strength $\hat{A}$ at $(x,y,z) = (-a,0,0)$ must be found such that one of the induced current loops will coincide with the dashed cylinder and thereby satisfy the boundary condition given by equation (27).

The current, $\underset{\sim}{J}_{tr}$, induced by the real coil is given by equation (16) which, for the present case, becomes

$$\underset{\sim}{J}_{tr} = -G_t\left[\underset{\sim}{i}\left(\frac{-y}{r^3}\right) + \underset{\sim}{j}\left(\frac{x-a}{r^3}\right)\right] \tag{32}$$

where

$$G_t = \sigma\omega m \sin \omega t$$

$$r^2 = (x-a)^2 + y^2 + z^2$$

and m is defined by equation (20). Therefore, a real stream function for $\underset{\sim}{J}_{tr}$ is

$$\psi_{tr} = -G_t[(x - a)^2 + y^2 + z^2]^{-1/2} \tag{33}$$

By trial and error, a stream function

$$\psi_{ti} = \mathbf{A}G_t[(x + a)^2 + y^2 + \mathbf{A}^2 z^2]^{-1/2} \tag{34}$$

was found for the image system so that the resultant stream function is

$$\psi_t = -G_t\{[(x - a)^2 + y^2 + z^2]^{-1/2} - \mathbf{A}[(x + a)^2 + y^2 + \mathbf{A}^2 z^2]^{-1/2}\} \tag{35}$$

and the total induced current becomes $\underset{\sim}{J}_t = \underset{\sim}{\nabla} \times \underset{\sim}{k}\psi_t$. This expression for ψ_t is particularly useful because the surface defined by the condition $\psi_t \equiv 0$ happens to be the cylindrical surface

$$\left[x - a\left(\frac{\mathbf{A}^2 + 1}{\mathbf{A}^2 - 1}\right)\right]^2 + y^2 = \left(\frac{2a\mathbf{A}}{\mathbf{A}^2 - 1}\right)^2 \tag{36}$$

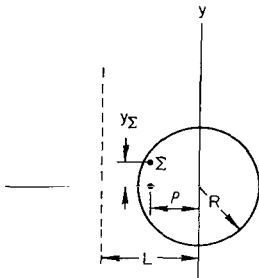so that the current loops corresponding to $\psi_t = 0$ meet the requirement specified by equation (27).

Figure 4.- Position of coils inside a cylindrical region.

Figure 4 illustrates the locations of the real primary and secondary Σ-coils after the y axis has been translated a distance $L = a(\mathbf{A}^2 + 1)/(\mathbf{A}^2 - 1)$, that is, to the center of the jet. Since $L - a = \rho$ and $R = 2a\mathbf{A}/(\mathbf{A}^2 - 1)$, a and $\mathbf{A}$ may be solved as functions of R and ρ with the result that

$$a = (R^2 - \rho^2)/2\rho \tag{37}$$

$$\mathbf{A} = R/\rho \tag{38}$$

If these expressions are substituted into equation (35) and if the y axis is translated a distance L, it follows that

$$\psi_t = -G_t[(\overline{x + \rho}^2 + y^2 + z^2)^{-1/2} - R(\overline{\rho x + R^2}^2 + \rho^2 y^2 + R^2 z^2)^{-1/2}] \tag{39}$$

Therefore, the final expression for the resultant current density vector is

$$\underset{\sim}{J}_t = \underset{\sim}{\nabla} \times \underset{\sim}{k}\psi_t$$

$$= -G_t \left\{ \underset{\sim}{i}\left[\frac{R\rho^2 y}{(\overline{\rho x + R^2}^2 + \rho^2 y^2 + R^2 z^2)^{3/2}} - \frac{y}{(\overline{x+\rho}^2 + y^2 + z^2)^{3/2}} \right] \right.$$

$$\left. - \underset{\sim}{j}\left[\frac{R\rho(\rho x + R^2)}{(\overline{\rho x + R^2}^2 + \rho^2 y^2 + R^2 z^2)^{3/2}} - \frac{x + \rho}{(\overline{x+\rho}^2 + y^2 + z^2)^{3/2}} \right] \right\} \qquad (40)$$

Equation (2) may now be used to obtain $\underset{\sim}{b}_t$ from the relation

$$\underset{\sim}{\nabla} \times \underset{\sim}{b}_t = \mu \underset{\sim}{J}_t \qquad (41)$$

by use of equation (11), of reference 23. That is, the perturbation field, $\underset{\sim}{b}_t$, at any field point (x',y',z') in the cylindrical plasma is given as

$$\underset{\sim}{b}_t(x',y',z',t) = \frac{\mu}{4\pi} \int_{-\infty}^{\infty} \int_{-R}^{R} \int_{-\sqrt{R^2-y^2}}^{\sqrt{R^2-y^2}} \underset{\sim}{J}_t(x,y,z,t) \times \underset{\sim}{\nabla} r^{-1} \, dx \, dy \, dz \qquad (42)$$

where $r = (\overline{x - x'}^2 + \overline{y - y'}^2 + \overline{z - z'}^2)^{1/2}$. Note that the current density vector $\underset{\sim}{J}_t$ does not vanish outside the cylindrical region as required by equation (26). However, this requirement is satisfied by equation (42) because the limits of integration do not extend beyond the cylindrical boundary so that the mathematical current loops outside the cylinder cannot contribute to $\underset{\sim}{b}_t$. Since the axis of the Σ-coil is parallel to $\underset{\sim}{k}$, only the z component of $\underset{\sim}{b}_t$ will be used in Faraday's law, equation (21). Since $(x',y',z') = (-\rho, y_\Sigma, y_\Sigma/\sqrt{2})$, the z component of $\underset{\sim}{b}_t$ must be

$$b_{zt} = \frac{\mu G_t}{4\pi} \int_{-\infty}^{\infty} \int_{-R}^{R} \int_{-\sqrt{R^2-y^2}}^{\sqrt{R^2-y^2}} \left\{ R\rho\left[\frac{\rho y(y - y_\Sigma) + (\rho x + R^2)(x+\rho)}{\left(\overline{x+\rho}^2 + \overline{y - y_\Sigma}^2 + \overline{z - \frac{y_\Sigma}{\sqrt{2}}}^2\right)^{3/2} \left(\overline{\rho x + R^2}^2 + \rho^2 y^2 + R^2 z^2\right)^{3/2}} \right] \right.$$

$$\left. - \left[\frac{y(y - y_\Sigma) + (x + \rho)^2}{\left(\overline{x+\rho}^2 + \overline{y - y_\Sigma}^2 + \overline{z - \frac{y_\Sigma}{\sqrt{2}}}^2\right)^{3/2} \left(\overline{x+\rho}^2 + y^2 + z^2\right)^{3/2}} \right] \right\} dx \, dy \, dz \qquad (43)$$

13

If the variables x, y, z and parameters ρ, y_Σ in the last equation are made dimensionless with respect to the jet radius R,

$$b_{zt} = \frac{\mu G_t}{4\pi R} \int_{-\infty}^{\infty} \int_{-1}^{1} \int_{-\sqrt{1-Y^2}}^{\sqrt{1-Y^2}} \left\{ \left[\frac{P^2 Y(Y-S) + P(X+P)(PX+1)}{\left(\overline{X+P}^2 + \overline{Y-S}^2 + \overline{Z-D}^2\right)^{3/2} \left(\overline{PX+1}^2 + P^2 Y^2 + Z^2\right)^{3/2}} \right] \right.$$

$$\left. - \left[\frac{Y(Y-S) + (X+P)^2}{\left(\overline{X+P}^2 + \overline{Y-S}^2 + \overline{Z-D}^2\right)^{3/2} \left(\overline{X+P}^2 + Y^2 + Z^2\right)^{3/2}} \right] \right\} dX\ dY\ dZ \qquad (44)$$

where $X = x/R$, $Y = y/R$, $Z = z/R$, $P = \rho/R$, $S = y_\Sigma/R$, and $D = S/\sqrt{2}$. Substitution of this expression into Faraday's law yields

$$\Phi_\Sigma = -(n_\Sigma r_\Sigma^2)(n_p r_p^2)(\mu\omega)^2 \frac{I_p \sigma \cos \omega t}{16R} \int_{-\infty}^{\infty} \int_{-1}^{1} \int_{-\sqrt{1-Y^2}}^{\sqrt{1-Y^2}} F_\Sigma\ dX\ dY\ dZ \qquad (45)$$

where F_Σ is used to denote the complicated integrand of the preceding expression. In order to eliminate the probe and coil characteristics, equation (45) is made dimensionless through division by equation (22) to obtain the desired correction factor

$$\frac{\Phi_\Sigma}{\Phi_{\Sigma\infty}} \equiv \Theta_\Sigma(S,P) = -\frac{3\sqrt{6}}{16\pi} S \int_{-\infty}^{\infty} \int_{-1}^{1} \int_{-\sqrt{1-Y^2}}^{\sqrt{1-Y^2}} F_\Sigma\ dX\ dY\ dZ \qquad (46)$$

For a given probe, the conductivity correction factor Θ_Σ represents the ratio of the Σ-coil signal that would be induced in a finite cylindrical region having a constant conductivity to the signal that would be induced in an infinite region having the same constant conductivity.

As might be anticipated, the integrals of equation (46) cannot be evaluated readily in closed form. Although one integration could be accomplished, it was more convenient to evaluate the integrals numerically rather than deal with the elliptic integrals resulting from the analytical integration. Therefore, equation (46) was computed using a numerical 10-point Gaussian-quadrature program written in Fortran IV and executed on an IBM 7090/7094 digital computer. (See ref. 21 for further details.) The results of the computation are presented in figure 5 which is a plot of Θ_Σ vs. $P = \rho/R$ for four practical values of the coil spacing parameter $S = y_\Sigma/R$; the dashed portions represent reasonable extrapolations of the computed curves. Additional points were not computed because each calculation of Θ_Σ consumed about one-half hour of computer time. However, the data reduction method presented in
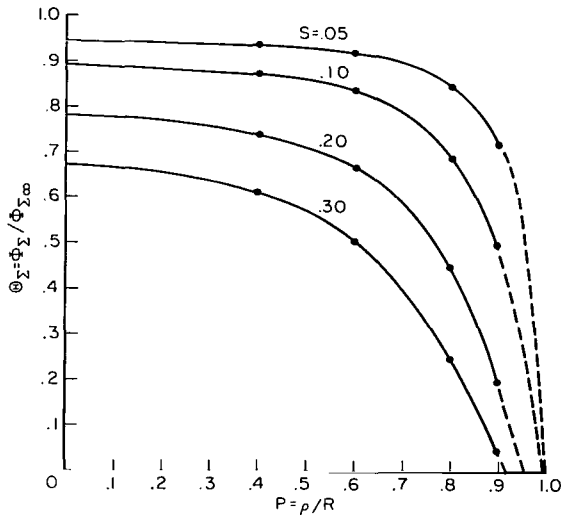
Figure 5.- Conductivity correction factor.

a subsequent section shows that satisfactory results can be achieved with the curves of figure 5. Values, rounded to two significant figures, are listed for convenience in table I.

The basic conductivity formula (eq. (24)) may now be modified to account for the presence of a cylindrical boundary by introducing the correction factor Θ_Σ with the result that

$$\sigma = \frac{\Phi_\Sigma C_\Sigma}{\Theta_\Sigma(S,P)} \qquad (47)$$

where C_Σ is a calibration constant to be determined by the methods outlined in reference 16. The last expression is still limited to the case of constant electrical conductivity.

TABLE I.- CONDUCTIVITY CORRECTION FACTORS, Θ_Σ

$P = \rho/R$	$S = y_\Sigma/R$						
	0.05	0.10	0.20	0.30	0.80	0.93	1.00
0.00	0.95	0.89	0.78	0.68	0.14	0.012	-0.05
.40	.94	.87	.74	.62	---	---	---
.60	.92	.83	.66	.51	---	---	---
.80	.85	.69	.44	.25	---	---	---
.90	.71	.47	.18	.044	---	---	---

Product of Conductivity and Velocity or $\sigma U_{||}$

Another application of the method of images yields a $\sigma U_{||}$ stream function $\psi_{||}$ such that

$$\psi_{||} = -G_{||}z\left\{\left[\overline{x+\rho}^2 + y^2 + z^2\right]^{-3/2} - R^3\left[\overline{\rho x + R^2}^2 + \rho^2 y^2 + R^2 z^2\right]^{-3/2}\right\} \qquad (48)$$

where $G_{||} = \sigma U_{||}m \cos \omega t$, and the y axis has been translated to the center of the stream as in figure 4. Using the stream function analogy explained above, one can derive the following expression for the current density vector:

15

$$\underset{\sim}{J}_{||} = -G_{||}z\left\{\left[3R^3\rho^2 y(\overline{\rho x + R^2}^2 + \rho^2 y^2 + R^2 z^2)^{-5/2} - 3y(\overline{x+\rho}^2 + y^2 + z^2)^{-5/2}\right]\underset{\sim}{i}\right.$$

$$\left. -\left[3R^3\rho\ \overline{\rho x+R^2}^2(\overline{\rho x+R^2}^2 + \rho^2 y^2 + R^2 z^2)^{-5/2} - 3(x+\rho)(\overline{x+\rho}^2 + y^2 + z^2)^{-5/2}\right]\underset{\sim}{j}\right\}$$

$$(49)$$

As was the case with $\underset{\sim}{b}_t$, $\underset{\sim}{b}_{||}$ is related to $\underset{\sim}{J}_{||}$ by the triple integral

$$\underset{\sim}{b}_{||}(x',y',z',t) = \frac{\mu}{4\pi}\int\int\int \underset{\sim}{J}_{||}(x,y,z,t) \times \underset{\sim}{\nabla}r^{-1}\ dx\ dy\ dz \qquad (50)$$

where $r = (\overline{x - x'}^2 + \overline{y - y'}^2 + \overline{z - z'}^2)^{1/2}$. Because the axis of the Y-coil is parallel to the y axis, only the $\underset{\sim}{j}$ component of $\underset{\sim}{b}_{||}$ will contribute to the induced electromotive force. That component, evaluated at $(x',y',z') = (-\rho,-y_\Sigma,0)$ and made dimensionless with respect to R, is

$$b_{y_{||}} = \frac{-3\mu G_{||}}{4\pi R^2}\int_{-\infty}^{\infty}\int_{-1}^{1}\int_{-\sqrt{1-Y^2}}^{\sqrt{1-Y^2}}\left[\frac{YZ^2}{(\overline{X+P}^2 + \overline{Y+S}^2 + Z^2)^{3/2}}\right]\times$$

$$\left[\frac{P^2}{(\overline{PX+1}^2 + P^2Y^2 + Z^2)^{5/2}} - \frac{1}{(\overline{X+P}^2 + Y^2 + Z^2)^{5/2}}\right]dX\ dY\ dZ$$

$$\equiv \frac{-3\mu G_{||}}{4\pi R^2}\int_{-\infty}^{\infty}\int_{-1}^{1}\int_{-\sqrt{1-Y^2}}^{\sqrt{1-Y^2}} F_Y\ dX\ dY\ dZ \qquad (51)$$

where F_Y represents the integrand.

Therefore, Faraday's law predicts that the potential Φ_Y induced at the Y-coil will be

$$\Phi_Y = -\left(n_Y r_Y^2\right)\left(n_p r_p^2\right)\sigma U_{||}\frac{3\omega I_p\mu^2}{16R^2}\sin\omega t\int\int\int F_Y\ dX\ dY\ dZ \qquad (52)$$

and, if this expression is divided by equation (23) to eliminate probe and coil characteristics,

$$\frac{\Phi_Y}{\Phi_{Y\infty}} \equiv \Theta_Y(S,P) = \frac{3S^2}{2\pi} \int_{-\infty}^{\infty} \int_{-1}^{1} \int_{-\sqrt{1-Y^2}}^{\sqrt{1-Y^2}} F_Y \; dX \; dY \; dZ \qquad (53)$$
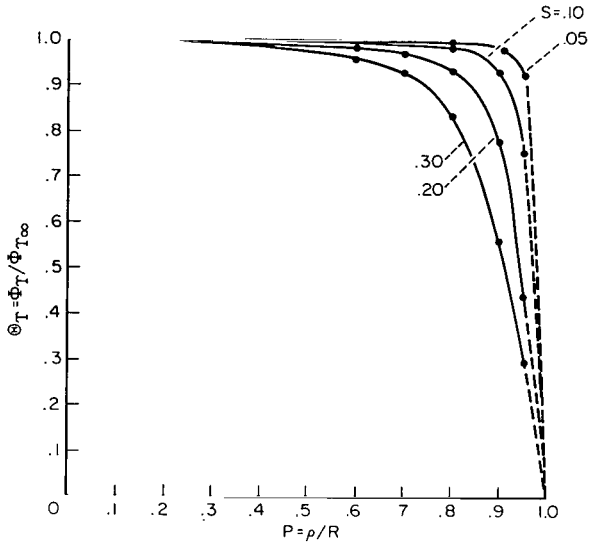

Figure 6.- Correction factor for $\sigma U_{||}$.

The correction factor Θ_Y defined by equation (53) is similar to the conductivity correction factor Θ_Σ because, for a given probe, Θ_Y represents the ratio of the Y-coil signal that would be induced in a finite cylindrical region having uniform values of σ and $U_{||}$ to the signal that would be induced in an infinite region having the same uniform values of σ and $U_{||}$. For convenience, this parameter will hereafter be referred to as the velocity correction factor even though it applies to the product $\sigma U_{||}$.

As with Θ_Σ, the integrations required by equation (53) were performed numerically on a digital computer using a program similar to that used for integrations in equation (46). The results are presented in figure 6 and are also listed, to two significant figures, in table II. The curves of figure 6 indicate that if $S \leq 0.10$, then the deviation of Θ_Y from unity is negligible except at the very edge of the cylindrical stream. As anticipated, the conductivity correction factors are more important than the velocity correction factors.

TABLE II.- VELOCITY CORRECTION FACTORS, Θ_Y

$P = \rho/R$	$S = y_\Sigma/R$					
	0.05	0.10	0.20	0.30	0.80	1.00
0.00	----	----	----	0.99	0.88	0.73
.60	---	---	0.99	.97	---	---
.70	----	----	.98	.93	---	---
.80	1.00	0.99	.94	.84	---	---
.90	.99	.94	.78	.55	---	---
.95	.93	.75	.44	.29		

Equation (25) may now be modified to include the velocity correction factor:

$$\sigma U_{||} = \frac{\Phi_\Upsilon C_\Upsilon}{\Theta_\Upsilon} \tag{54}$$

where C_Υ is a calibration constant. Equation (54) is still limited to a conducting fluid having a cylindrical boundary, uniform σ, and uniform $U_{||}$.

The conductivity correction factors presented in figure 5 were verified experimentally using a three-coil probe. (This experiment was performed with the aid of Mr. R. E. Posch.) Each of two plexiglas cylinders having different diameters was filled with an electrolyte having a conductivity of 74.8 mho/meter. Then the radial variation of the Σ-coil output was recorded for each cylinder. The results were normalized with respect to an experimentally determined value of $\Phi_{\Sigma\infty}$ (see ref. 16 for details) to obtain Θ_Σ. In figure 7 the experimental values of Θ_Σ are compared with theoretical values computed from the curves of figure 5. The differences are less than 10 percent except near the edge where the output of the Σ-coil was very small and was extremely sensitive to the alinement of the probe's axis parallel to the z axis of the cylinder.

The probe was also placed immediately adjacent to and outside each cylinder wall (in room air) to record the magnitude of the signal produced by the currents induced in the electrolyte by the primary dipole field, $\underset{\sim}{B}_p$. As indicated by the data points at $P = 1.025$ and $P = 1.10$, the result was that the signals were too small to be observed on the oscilloscope at its maximum sensitivity setting; that is, the induced signals were at least ten times smaller than any signals obtained inside the cylinders. Now, in a free plasma jet it is reasonable to assume that the conductivity increases from zero at the edge to a maximum that occurs at or near the center line. The result of the experiment indicates that when the probe is swept through the jet, the signal induced on the Σ-coil at a given radial position, say $\rho = \rho_0$, is not significantly influenced by the increased conductivity in the region $0 \leq \rho \leq \rho_0$; consequently, Φ_Σ is primarily a function of the variable conductivity in the region $\rho_0 \leq \rho \leq R$. This observation is of fundamental importance to the data reduction technique presented in the next section.

Figure 7.- Comparison of theoretical curves with experimental measurements in cylinders of acid.

A METHOD FOR COMPUTING CONDUCTIVITY AND VELOCITY PROFILES
OF AXISYMMETRIC PLASMA JETS

   In this section a method for computing conductivity and velocity profiles is presented and applied to data taken by a three-coil probe in a constricted-arc wind tunnel. The method is based on the premise that the continuously varying profile can be approximated by a number of steps as suggested in figure 8. It is then assumed that each level can be treated as a cylinder of constant conductivity (or constant $\sigma U_{\parallel}$) by the theory developed above. As noted at the end of the last section, the magnitudes of Φ_{Σ} and Φ_{Y} are negligible when the probe is outside a cylinder of conducting fluid. Hence, if the analysis of a given profile is started at the outside boundary of a jet, the calculations can proceed to the center in an explicit fashion so that all parameters are known as each step is made inward. As illustrated in figure 8, the cylindrical plasma jet is, as a first approximation, subdivided into a finite number, n, of concentric cylindrical regions each having a different, but constant conductivity. The upper part of the sketch shows a cross-section of the jet and the lower part displays a typical Φ_{Σ}-trace together with the n-step approximation of the actual continuously varying conductivity profile.
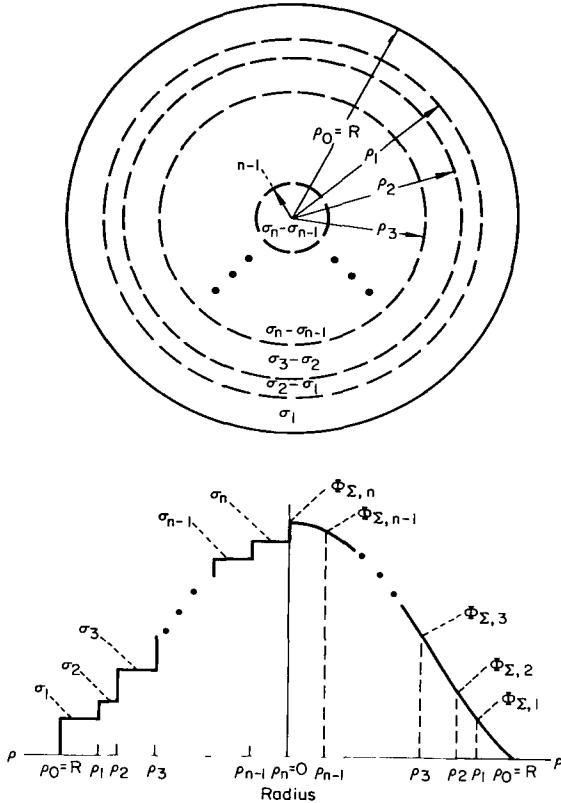
   When the probe is located at the radial position $\rho = \rho_1$ shown in figure 8, the two data points on the abscissa axis of figure 7 indicate that the influence of the increased conductivity in the inner regions has a negligible effect on the value of $\Phi_{\Sigma,1}$. Therefore, $\Phi_{\Sigma,1}$ may be interpreted as the signal which results from placing the probe at a radius ρ_1 in a cylindrical region of radius ρ_0 containing a fluid of conductivity σ_1. The signal $\Phi_{\Sigma,2}$ results from placing the probe simultaneously at a radius $\rho = \rho_2$ in two cylindrical regions of radii ρ_0 and ρ_1 containing, respectively, fluids of conductivity σ_1 and $\sigma_2 - \sigma_1$. Similarly, $\Phi_{\Sigma,3}$ is caused by the simultaneous immersion of the probe at a radius $\rho = \rho_3$ in three cylindrical regions of radii ρ_0, ρ_1, and ρ_2 containing, respectively, fluids of conductivity σ_1, $\sigma_2 - \sigma_1$, and $\sigma_3 - \sigma_2$. The extension of this

Figure 8.- Measured profile subdivided to apply boundary corrections.

reasoning to $\Phi_{\Sigma,n}$ is straightforward and the results may be put into mathematical form by the following set of n linear equations in n unknowns:

$$\Phi_{\Sigma,1} = \frac{\sigma_1}{C_\Sigma} \Theta_\Sigma\left(\frac{y_\Sigma}{\rho_o} \; , \; \frac{\rho_1}{\rho_o}\right)$$

$$\Phi_{\Sigma,2} = \frac{\sigma_1}{C_\Sigma} \Theta_\Sigma\left(\frac{y_\Sigma}{\rho_o} \; , \; \frac{\rho_2}{\rho_o}\right) + \frac{\sigma_2 - \sigma_1}{C_\Sigma} \Theta_\Sigma\left(\frac{y_\Sigma}{\rho_1} \; , \; \frac{\rho_2}{\rho_1}\right)$$

$$\Phi_{\Sigma,3} = \frac{\sigma_1}{C_\Sigma} \Theta_\Sigma\left(\frac{y_\Sigma}{\rho_o} \; , \; \frac{\rho_3}{\rho_o}\right) + \frac{\sigma_2 - \sigma_1}{C_\Sigma} \Theta_\Sigma\left(\frac{y_\Sigma}{\rho_1} \; , \; \frac{\rho_3}{\rho_1}\right) + \frac{\sigma_3 - \sigma_2}{C_\Sigma} \Theta_\Sigma\left(\frac{y_\Sigma}{\rho_2}, \frac{\rho_3}{\rho_2}\right)$$

$$\vdots \qquad\qquad \vdots \qquad\qquad\qquad \vdots \qquad\qquad\qquad \vdots \tag{55}$$

$$\Phi_{\Sigma,n-1} = \sum_{i=o}^{n-2} \left[\frac{\sigma_{i+1} - \sigma_i}{C_\Sigma}\right] \Theta_\Sigma\left(\frac{y_\Sigma}{\rho_i} \; , \; \frac{\rho_{n-1}}{\rho_i}\right) ,$$

$$\Phi_{\Sigma,n} = \sum_{i=o}^{n-1} \left[\frac{\sigma_{i+1} - \sigma_i}{C_\Sigma}\right] \Theta_\Sigma\left(\frac{y_\Sigma}{\rho_i} \; , \; 0\right) , \qquad n \geq 2$$

In these equations C_Σ represents the conductivity calibration constant, σ_o is identically zero, and the argument of Θ_Σ is given, respectively, in terms of the parameters $S = y_\Sigma/R$, and $P = \rho/R$. After inserting values for Θ_Σ from figure 5, these simultaneous equations may be solved for σ_i, $i = 1, \ldots, n$.

The same technique may be applied to obtain a $\sigma U_{||}$ profile and the equations that must be solved for an n-step approximation are:

$$\Phi_{Y,1} = \frac{[\sigma U_{||}]_1}{C_Y} \, \Theta_Y\!\left(\frac{y_\Sigma}{\rho_o} \, , \, \frac{\rho_1}{\rho_o}\right)$$

$$\Phi_{Y,2} = \frac{[\sigma U_{||}]_1}{C_Y} \, \Theta_Y\!\left(\frac{y_\Sigma}{\rho_o} \, , \, \frac{\rho_2}{\rho_o}\right) + \frac{[\sigma U_{||}]_2 - [\sigma U_{||}]_1}{C_Y} \, \Theta_Y\!\left(\frac{y_\Sigma}{\rho_1} \, , \, \frac{\rho_2}{\rho_1}\right)$$

$$\Phi_{Y,3} = \frac{[\sigma U_{||}]_1}{C_Y} \, \Theta_Y\!\left(\frac{y_\Sigma}{\rho_o} \, , \, \frac{\rho_3}{\rho_o}\right) + \frac{[\sigma U_{||}]_2 - [\sigma U_{||}]_1}{C_Y} \, \Theta_Y\!\left(\frac{y_\Sigma}{\rho_1} \, , \, \frac{\rho_3}{\rho_1}\right)$$

$$+ \frac{[\sigma U_{||}]_3 - [\sigma U_{||}]_2}{C_Y} \, \Theta_Y\!\left(\frac{y_\Sigma}{\rho_2} \, , \, \frac{\rho_3}{\rho_2}\right) \tag{56}$$

$$\vdots \qquad \vdots \qquad \vdots \qquad \vdots \qquad \vdots \qquad \vdots$$

$$\Phi_{Y,n-1} = \sum_{i=o}^{n-2} \frac{[\sigma U_{||}]_{i+1} - [\sigma U_{||}]_i}{C_Y} \, \Theta_Y\!\left(\frac{y_\Sigma}{\rho_i} \, , \, \frac{\rho_{n-1}}{\rho_i}\right) ,$$

$$\Phi_{Y,n} = \sum_{i=o}^{n-1} \frac{[\sigma U_{||}]_{i+1} - [\sigma U_{||}]_i}{C_Y} \, \Theta_Y\!\left(\frac{y_\Sigma}{\rho_i} \, , 0\right) , \qquad n \geq 2$$

where C_Y is the velocity calibration constant, $[\sigma U_{||}]_o$ is identically zero, and the values for Θ_Y as functions of $S = y_\Sigma/R$ and $P = \rho/R$ are given in figure 6. The solutions of equations (55) and (56) may then be combined to obtain an n-step approximation of the $U_{||}$ profile. As the number of subdivisions is increased, subject to the limitations to be discussed below, the discontinuous step profiles should approach the actual continuously varying profiles.

The data reduction technique may be divided into three parts as follows:

1. The edge of the jet may be determined from the Σ-coil output provided that the response time of the probe is known. The response time of a probe system may be determined from a consideration of superimposed data taken during a two-way sweep through the plasma stream. Using this technique, Rossow and Posch reported a response time of 0.03 second. Figure 9 is a typical data record obtained by Rossow and Posch with a three-coil probe $(S = y_\Sigma/R = 0.234)$ in a constricted-arc wind tunnel having an arc current $I_{arc} = 200$ A and the conductivity data (lower trace) indicate that the
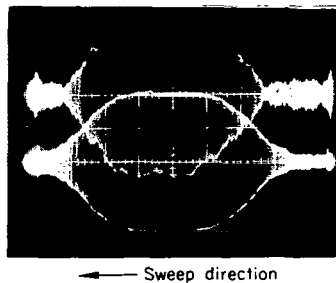
Scope sensitivity settings:

T (.02 mv/cm)

Σ (.05 mv/cm)

◄──── Sweep direction

Figure 9.- Data record.

extreme radius of the jet was about 9.5 cm. To assess the sensitivity of the data reduction method to the magnitude of the jet radius, profiles were computed for three radii: 9.0 cm, 9.5 cm, and 10.0 cm; the corrected center line values of σ and $U_{||}$ for the three cases did not differ by more than 10 percent. Therefore, by contrast with the measurement technique of Donskoi, et al. (ref. 7), the accuracy of this method is not highly dependent on a precise determination of the jet radius.

2. The null signal should be added to the Φ_Σ trace and subtracted from the Φ_Y trace; reasons for this procedure are discussed below. Then, peak-to-peak values of Φ_Σ and Φ_Y may be plotted vs. radial position of the instrument; the radial position should be adjusted to compensate for the response time of the system. A mean value for the Φ_Y curve is used, thereby eliminating the local signal excursions caused by random stream noise.

3. The next step is to subdivide the cylindrical jet into subregions as suggested by figure 8 and to apply equations (55) and (56) to the Φ_Σ and Φ_Y data. It is suggested that this step be repeated several times in order to test its accuracy; that is, as a first approximation, use three subregions to obtain three-step σ and $U_{||}$ profiles. Then, as a second approximation, use four subregions for the computation. Additional approximations obtained by increasing the number of subdivisions can be carried out to increase the accuracy and definition of the curves. A limitation on the maximum number of subdivisions is discussed below.

The velocity trace of figure 9 indicates a minimum signal at about 2.8 cm from the center of the oscilloscope screen. This phenomenon is due to $b_{||}$ and B_p being $180°$ out of phase as indicated by equations (14) and (19). Outside the stream Φ_Y is nonzero because the actual B_p differs slightly from the theoretical B_p. As the probe nears the edge of the stream, the magnitude of $b_{||}$ increases and causes Φ_Y, which is proportional to $B_p + b_{||}$, to decrease because of the $180°$-phase difference. As the probe sweep continues into the jet, the magnitude of $b_{||}$ dominates and Φ_Y begins to increase. Therefore, when the data are reduced, the Φ_Y ordinates should be increased by the value of the null signal while the Φ_Σ ordinates should be decreased by the value of the null signal.

If the above data reduction technique is applied to the Φ_Σ and Φ_Y signals of figure 9, then the result is given by figure 10. The dashed curves in that figure represent profiles which were not corrected for the presence of a cylindrical boundary and are based on the application of equations of the form

$$\frac{\sigma}{\Phi_\Sigma} = C_\Sigma \qquad \text{and} \qquad \frac{\sigma U_{||}}{\Phi_\Upsilon} = C_\Upsilon$$

to center-line values of Φ_Σ and Φ_Υ. The uncorrected $U_{||}$ profile was obtained by dividing the dashed ordinates of the $\sigma U_{||}$ profile by the dashed ordinates of the σ profile. As anticipated, the conductivity correction factor Θ_Σ had a greater influence on the reduction of data than did the velocity correction factor Θ_Υ. In fact, the example presented in figure 10
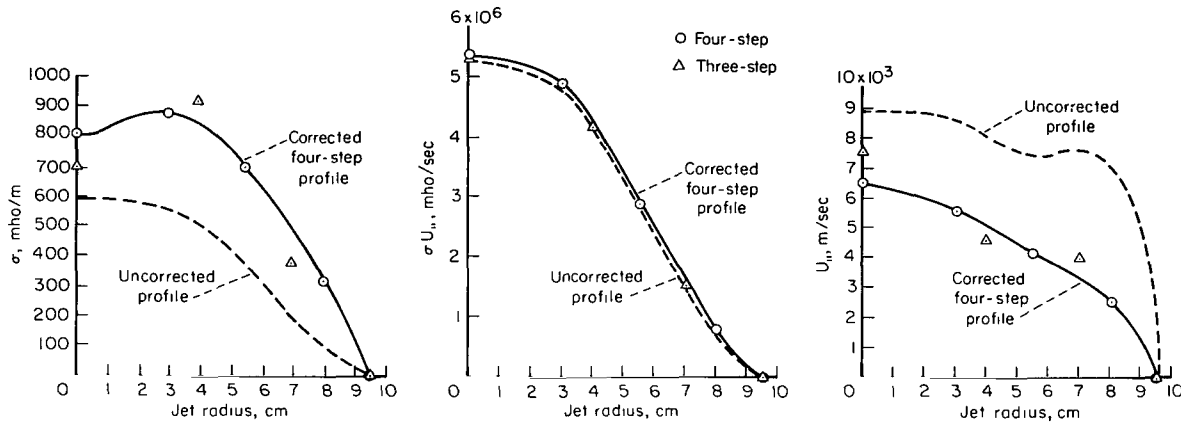

Figure 10.- Electrical conductivity and velocity profiles, based on the data of figure 9, in a free argon plasma jet.

indicates that the corrections of the $\sigma U_{||}$ profile are negligible. However, because of the conductivity corrections, the corrected $U_{||}$ profile may differ considerably from the uncorrected $U_{||}$ profile.

As mentioned above, the choice of subregions is not completely arbitrary and it was found that the values of y_Σ and R impose two important restrictions. The first restriction may be explained by the curves of figure 11. Consider a fluid having a cylindrical boundary and, for example, a constant conductivity of 888 mho/m. Suppose that an oscilloscope recording is made of Φ_Σ vs. radial position, ρ, for this fluid. Then, if the correct Φ_Σ values are substituted into the formula

$$\frac{\sigma}{\Phi_\Sigma} = \frac{C_\Sigma}{\Theta_\Sigma(y_\Sigma/R, \rho/R)}$$

for different values of ρ, the horizontal curve marked σ_{true} will be the result. However, the smallest screen division for many oscilloscopes is 2 mm and, with the presence of a slight amount of noise, it is possible to err by as much as 1 mm when reading the oscilloscope data record. Therefore, a typical scope sensitivity setting of 0.05 mV/cm, a calibration constant of 3000 mho/m--mV from reference 16, and the above equation were used to compute
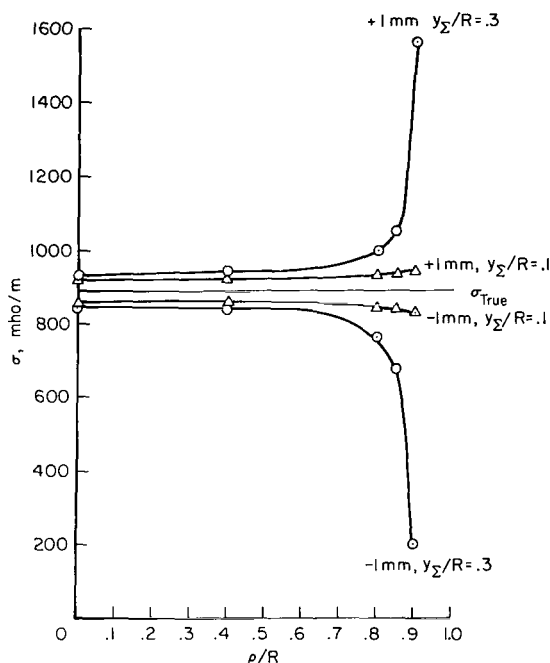
23
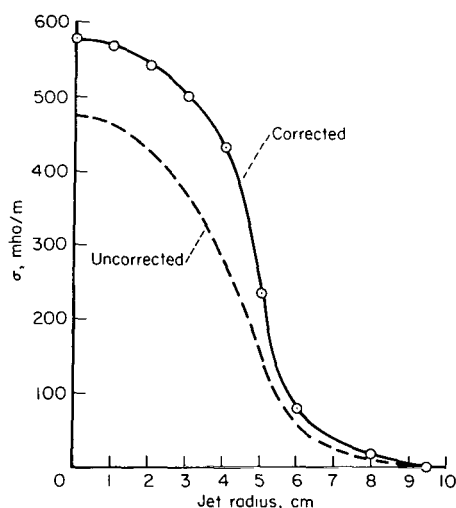
Figure 11.- Uncertainty resulting from reading error.

Figure 12.- Conductivity profile in an argon plasma jet.

the error curves of figure 11 for two different values of the parameter y_Σ/R. The figure shows that a reading error of 1 mm can cause a large error in σ when $y_\Sigma/R = 0.3$ and $\rho/R \geq 0.80$. However, the error is more moderate when $y_\Sigma/R = 0.10$.

Thus, if y_Σ/R is small, the stream can be subdivided into several subregions without risking the introduction of a large oscilloscope reading error. The σ profile of figure 12 illustrates this principle. The corrected σ profile, using data recorded with a probe such that $S = 0.085$, was computed on the basis of nine subregions whereas only four subregions were used for the profile of figure 10 ($S = 0.234$) because it was found that further subdivision introduced large uncertainty errors. It is also interesting, though not surprising, that the smaller the value of y_Σ/R, the smaller the resulting corrections.

The other restriction concerns the choice of the radius, ρ_{n-1} of the innermost subregion. It is obvious that ρ_{n-1} must satisfy the inequality $\rho_{n-1} \geq y_\Sigma$. Experience indicates that ρ_{n-1} should be chosen so that $\rho_{n-1} \geq 1.14 \, y_\Sigma$. This restriction on the value of ρ_{n-1} places a lower limit of approximately 0.10 on the correction factor Θ_Σ. Smaller values of this factor would magnify oscilloscope reading errors by an intolerable amount.

It is difficult to estimate the overall accuracy of the preceding data-reduction technique. The uncertainty resulting from the presence of random electromagnetic noise or oscilloscope reading errors has already been discussed. Another possible error source is the neglect of

axial variations in σ and $U_\parallel$. However, the magnitude of such an error is probably small because the magnitudes of the theoretical current vectors, $\underset{\sim}{J}_t$ and $\underset{\sim}{J}_\parallel$, decrease rapidly in the axial direction and because the effects of the higher upstream values of σ and $U_\parallel$ may be canceled by the lower downstream values. If the plasma stream is steady and fairly free from random electromagnetic noise, the data reduction technique presented in this section probably yields center-line values differing from the true values by no more than 20 percent.

To test the validity of dividing the stream into several regions of constant σ, an experiment was performed using H_2SO_4 solutions in plastic cylinders. The test was performed in the three concentric plexiglas cylinders as sketched in the plan view of figure 13; the center-line position of the instrument is shown with the axis of the probe parallel to the z axis of the cylinders. The depth of each cylinder was at least 18 cm because tests indicated that this value simulated a cylinder of infinite extent. All plexiglas walls were 4.7 mm thick and the inside radii of the cylinders were 5.95 cm, 9.77 cm, and 12.3 cm as indicated in figure 13. The center cylinder was filled with a sulphuric acid solution having a conductivity of 74.8 mho/m as determined by a conductivity cell measurement. Similarly, the two annular spaces were filled with acid solutions having conductivities of 49 and 29 mho/m.
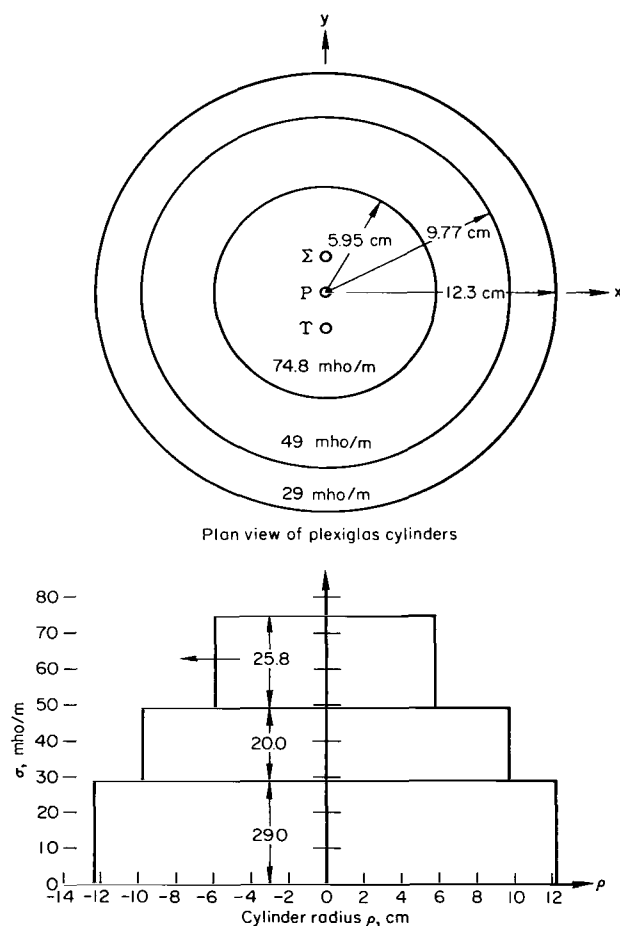
It was found that the center-line value of Φ_Σ could be predicted from the theory given above if the probe were considered to be immersed simultaneously at the center of three cylinders of radii 12.3 cm, 9.77 cm, and 5.95 cm containing electrolytes of conductivity 29, 20, and 25.8 mho/m, respectively. Then equation (47),

$$\frac{\sigma}{\Phi_\Sigma} = \frac{1585}{\Theta_\Sigma(S,P)} \qquad \text{mho/m-mV}$$

could be used to compute the contribution of the currents induced in each cylinder to the total probe output; for the instrument used in

Plan view of plexiglas cylinders

Figure 13.- Conductivity measured in acid solutions.

this experiment, the conductivity calibration constant was 1585 mho/m-mV. Using the correction factors given in figure 5 and setting y_Σ = 2.22 cm, one may calculate the probe output as follows:

$$\Phi_\Sigma = \frac{1}{1585} \left[29\Theta_\Sigma\left(\frac{2.22}{12.3} , 0\right) + 20\Theta_\Sigma\left(\frac{2.22}{9.77} , 0\right) + 25.8\Theta_\Sigma\left(\frac{2.22}{5.95} , 0\right) \right]$$

$$= \frac{1}{1585} \left[29 \times 0.805 + 20 \times 0.753 + 25.8 \times 0.602 \right]$$

$$= 0.0338 \text{ mV}$$

This theoretical value agrees quite well with the experimental value of 0.034 mV. The off-axis experimental values of Φ_Σ for the case $\rho \neq 0$ could not be predicted by the theory because the two inner plexiglas walls created rather complicated boundary conditions.

CONCLUDING REMARKS

Tests in concentric cylinders filled with acid solutions furnished reasonable confirmation of the conductivity correction factors that were used to correct the raw conductivity data for the existence of a boundary and for cross-stream σ variations. Using $\sigma U_{\parallel}$ correction factors, the method was extended to raw $\sigma U_{\parallel}$ data and the corrected σ and $\sigma U_{\parallel}$ profiles were used to compute a velocity profile.

Although these results indicate that the present design has the advantages of practicality and theoretical justification, some additional development is needed. Specifically, the following items should be investigated.

1. A new probe that permits variation of y_Σ should be constructed and tested for several values of $2\rho_0/y_\Sigma$ under identical plasma stream conditions and the corrected data from these tests should be analyzed to determine the significance of this parameter. It is believed that this parameter is a measure of the magnitude of mutual flow disturbance effects between adjacent support rods.

2. An oscillator having several output frequencies should be used with the probe to evaluate the importance of the frequency, ω, of the impressed power.

3. Improvement of the response time of the instrument system should be attempted.

4. Other materials, such as precision quartz tubing, should be tested for coil support rods.

5. A suitable experimental method for determining the $\sigma U_{||}$ calibration constant C_Y should be devised.

6. The use of the voltages Φ_Z and Φ_Y to produce, by means of electronic division, a signal that is linearly proportional to $U_{||}$. An alternate probe system (primary and two fore and aft secondary coils located on the z axis; also, the axis of each coil alined with the z axis) should be investigated because a single support rod containing three coils would perturb a plasma stream far less than a probe having three separate coil support rods.

Ames Research Center
    National Aeronautics and Space Administration
        Moffett Field, Calif., 94035, Nov. 14, 1967
            125-24-03-02-00-21

REFERENCES

1. Lin, S. C.; Resler, E. L.; and Kantrowitz, Arthur: Electrical Conductivity of Highly Ionized Argon Gases Produced by Shock Waves. J. Appl. Phys., vol. 26, no. 1, 1955, pp. 95-109.

2. Persson, K. B.: A Method for Measuring the Conductivity in a High Electron Density Plasma. J. Appl. Phys., vol. 32, no. 12, 1961, pp. 2631-2640.

3. Koritz, H. E.; and Keck, J. C.: Technique for Measuring the Electrical Conductivity of Wakes of Projectiles at Hypersonic Speeds. Rev. Sci. Instr., vol. 35, no. 2, 1964, pp. 201-208.

4. Olson, R. A.; and Lary, E. C.: Electrodeless Plasma Conductivity Probe Apparatus. Rev. Sci. Instr., vol. 33, no. 12, 1962, pp. 1350-1353.

5. Stubbe, E. J.: A Measurement of the Electrical Conductivity of Plasmas. AIAA Preprint 66-181, 1966.

6. Blackman, V. H.: Magnetohydrodynamic Flow Experiment of a Steady State Nature. ARS Preprint 1007-59, 1959.

7. Donskoi, K. V.; Dunaev, Yu. A.; and Prokof'ev, I. A.: Measurement of Electrical Conductivity in Gas Streams. Soviet Phys. - Tech. Phys., vol. 7, 1963, pp. 805-807.

8. Akimov, A. V.; and Konenko, O. R.: Measurement of Plasma Conductivity by a Radio-Frequency Method. Soviet Phys. - Tech. Phys., vol. 10, 1966, pp. 1126-1127.

9. Tanaka, Hiroshi; and Hagi, Mikiko: A Method of Measurement of Plasma Conductivity. II. Example of Measurement. Japanese J. Appl. Phys., vol. 3, 1964, pp. 338-341.

10. Savic, P.; and Boult, G. T.: A Frequency Modulation Circuit for the Measurement of Gas Conductivity and Boundary Layer Thickness in a Shock Tube. J. Sci. Instr., vol. 39, 1962, pp. 258-266.

11. Luther, Alan H.: A Non-Uniform-Plasma, Electrical Conductivity Probe. TR 63-165, U.S. Naval Ordnance Laboratory, White Oak, Md., Aug. 30, 1963.

12. Fuhs, A. E.: An Instrument to Measure Velocity-Electrical Conductivity of Arc Plasmajets. AIAA J., vol. 2, 1964, pp. 667-673.

13. Poberezhskii, L. P.: Measurement of Electrical Conductivity of Gas Jets. Soviet Phys. - Tech. Phys., vol. 8, 1964, pp. 1092-1094.

14. Poberezhskii, L. P.: Measurement of Velocity and Electrical Conductivity of an Ionized Gas Stream. Soviet Phys. - Tech. Phys., vol. 8, 1964, pp. 1088-1092.

15. Hollister, Donald D.: A Technique for the Experimental Determination of the Electrical Conductivity of Plasmas. AIAA J., vol. 2, no. 9, 1964, pp. 1568-1571.

16. Rossow, V. J.; and Posch, R. E.: Coil Systems for Measuring Conductivity and Velocity of Plasma Streams. Rev. Sci. Instr., vol. 37, no. 9, 1966, pp. 1232-1242.

17. Carter, A. F.; McFarland, D. R.; Weaver, W. R.; Park, S. K.; and Wood, G. P.: Operating Characteristics, Velocity, and Pitot Distribution and Material Evaluation Tests in the Langley One-In.-Square Plasma Accelerator. AIAA Preprint 66-180, 1966.

18. Stine, H. A.; Watson, V. R.; and Shepard, C. E.: Effect of Axial Flow on the Behavior of the Wall-Constricted Arc. Agardograph 84, pt. 1, Sept. 1964, pp. 451-485.

19. Gottschlich, Chad F.; Enright, John A.; and Cadek, F. C.: Measurement of the Velocity Distribution in a Plasmajet. AIAA J., vol. 4, 1966, pp. 1085-1087.

20. Clayden, W. A.: Langmuir Probe and Velocity Measurements in the ARDE Plasma Jet. Agardograph 68, MacMillan, N. Y., 1964, pp. 419-446.

21. Vendell, Edward W.: Boundary Corrections for a Three-Coil Conductivity/Velocity Plasma Probe. Ph.D. Thesis, School of Mechanical Engineering, Oklahoma State University, Stillwater, Oklahoma, 1967.

22. Rossow, V. J.: On Series Expansions in Magnetic Reynolds Number. NASA TN D-10, 1959.

23. Stratton, J. A.: Electromagnetic Theory. McGraw-Hill, N. Y., 1941.

24. Jackson, J. D.: Classical Electrodynamics. John Wiley and Sons, Inc., N. Y., 1962.

"The aeronautical and space activities of the United States shall be conducted so as to contribute . . . to the expansion of human knowledge of phenomena in the atmosphere and space. The Administration shall provide for the widest practicable and appropriate dissemination of information concerning its activities and the results thereof."

—NATIONAL AERONAUTICS AND SPACE ACT OF 1958

NASA SCIENTIFIC AND TECHNICAL PUBLICATIONS

TECHNICAL REPORTS: Scientific and technical information considered important, complete, and a lasting contribution to existing knowledge.

TECHNICAL NOTES: Information less broad in scope but nevertheless of importance as a contribution to existing knowledge.

TECHNICAL MEMORANDUMS: Information receiving limited distribution because of preliminary data, security classification, or other reasons.

CONTRACTOR REPORTS: Scientific and technical information generated under a NASA contract or grant and considered an important contribution to existing knowledge.

TECHNICAL TRANSLATIONS: Information published in a foreign language considered to merit NASA distribution in English.

SPECIAL PUBLICATIONS: Information derived from or of value to NASA activities. Publications include conference proceedings, monographs, data compilations, handbooks, sourcebooks, and special bibliographies.

TECHNOLOGY UTILIZATION PUBLICATIONS: Information on technology used by NASA that may be of particular interest in commercial and other non-aerospace applications. Publications include Tech Briefs, Technology Utilization Reports and Notes, and Technology Surveys.

Details on the availability of these publications may be obtained from:

SCIENTIFIC AND TECHNICAL INFORMATION DIVISION

NATIONAL AERONAUTICS AND SPACE ADMINISTRATION

Washington, D.C. 20546